



**HAL**  
open science

## Early stages of core segregation recorded by Fe isotopes in an asteroidal mantle

J. A. Barrat, O. Rouxel, K. Wang, F. Moynier, A. Yamaguchi, A. Bischoff, J.  
Langlade

► **To cite this version:**

J. A. Barrat, O. Rouxel, K. Wang, F. Moynier, A. Yamaguchi, et al.. Early stages of core segregation recorded by Fe isotopes in an asteroidal mantle. *Earth and Planetary Science Letters*, 2015, 419, pp.93-100. 10.1016/j.epsl.2015.03.026 . insu-03579972

**HAL Id: insu-03579972**

**<https://insu.hal.science/insu-03579972>**

Submitted on 18 Aug 2023

**HAL** is a multi-disciplinary open access archive for the deposit and dissemination of scientific research documents, whether they are published or not. The documents may come from teaching and research institutions in France or abroad, or from public or private research centers.

L'archive ouverte pluridisciplinaire **HAL**, est destinée au dépôt et à la diffusion de documents scientifiques de niveau recherche, publiés ou non, émanant des établissements d'enseignement et de recherche français ou étrangers, des laboratoires publics ou privés.

## Early stages of core segregation recorded by Fe isotopes in an asteroidal mantle

Barrat Jean-Alix <sup>1,\*</sup>, Rouxel Olivier <sup>2</sup>, Wang K. <sup>3</sup>, Moynier F. <sup>4,5</sup>, Yamaguchi A. <sup>6,7</sup>, Bischoff A. <sup>8</sup>, Langlade Jessica <sup>9</sup>

<sup>1</sup> Univ Bretagne Occidentale, CNRS, UMR 6538, Inst Univ Europeen Mer, F-29280 Plouzane, France.

<sup>2</sup> IFREMER, Ctr Brest, F-29280 Plouzane, France.

<sup>3</sup> Harvard Univ, Dept Earth & Planetary Sci, Cambridge, MA 02138 USA.

<sup>4</sup> Univ Paris Diderot, Inst Univ France, Inst Phys Globe Paris, Sorbonne Paris Cite, F-75238 Paris 05, France.

<sup>5</sup> Inst Univ France, Paris, France.

<sup>6</sup> Natl Inst Polar Res, Tachikawa, Tokyo 1908518, Japan.

<sup>7</sup> Grad Univ Adv Sci, Sch Multidisciplinary Sci, Dept Polar Sci, Tachikawa, Tokyo 1908518, Japan.

<sup>8</sup> Univ Munster, Inst Planetol, D-48149 Munster, Germany.

<sup>9</sup> CNRS, UMS 3113, IUEM, F-29280 Plouzane, France.

\* Corresponding author : Jean-Alix Barrat, email address : [barrat@univ-brest.fr](mailto:barrat@univ-brest.fr)

### Abstract :

Ureilite meteorites are achondrites that are debris of the mantle of a now disrupted differentiated asteroid rich in carbon. They provide a unique opportunity to study the differentiation processes of such a body. We analyzed the iron isotopic compositions of 30 samples from the Ureilite Parent Body (UPB) including 29 unbrecciated ureilites and one ureilitic trachyandesite (ALM-A) which is at present the sole large crustal sample of the UPB. The  $\delta^{56}\text{Fe}$  of the whole rocks fall within a restricted range, from 0.01 to 0.11‰, with an average of  $+0.056 \pm 0.008$ ‰, which is significantly higher than that of chondrites. We show that this difference can be ascribed to the segregation of S-rich metallic melts at low degrees of melting at a temperature close to the Fe–FeS eutectic, and certainly before the onset of the melting of the silicates (View the MathML source <1100°C), in agreement with the marked S depletions, and the siderophile element abundances of the ureilites. These results point to an efficient segregation of S-rich metallic melts during the differentiation of small terrestrial bodies.

### Highlights

► Ureilites displays  $\delta^{56}\text{Fe}$  values higher than average chondrite. ► Segregation of Fe-sulfide melts explains the high  $\delta^{56}\text{Fe}$  values in ureilites. ► Formation of a core can begin at very low degrees of melting through the circulation of a Fe–S melt through a silicate mantle.

---

**Keywords** : iron isotopes, achondrite, ureilite, core

# 1. Introduction

51           One of the most significant issues for understanding the differentiation of telluric bodies is  
52 when and how their cores formed. Trace element abundances and W isotopic compositions obtained  
53 on a series of iron meteorites indicate that the cores in the first differentiated planetesimals aggregated  
54 metallic melts with various S contents, and formed from ca. 0.6 to 3 Myrs after the first solids  
55 condensed in the Solar System (e.g., Blichert-Toft et al., 2010; Kruijer et al., 2014 and references  
56 therein). The mechanisms of core formation are still highly debated, especially for the early stages of  
57 the process. The percolation of Fe-S melts into an olivine matrix has been suggested and  
58 experimentally investigated, but the contribution of such melts to the cores of the planetary embryos or  
59 of larger bodies, is a matter of debate (Bruhn et al., 2000; Yoshino et al., 2003; Bagdassarov et al.,  
60 2009; Rushmer and Petford, 2011; Watson and Roberts, 2011). However, important constraints on the

61 early stages of the differentiation of some small bodies are potentially recorded in their mantles, which  
62 can be investigated using meteorite samples.

63 Ureilites are remnants of the mantle of a now-disrupted carbon-rich body (Downes et al.,  
64 2008), and are among the most common achondrites in the meteorite collections (about 400 ureilites  
65 are currently reported in the Meteoritical Bulletin Database). They are ultramafic achondrites (e.g.,  
66 Mittlefehldt et al., 1998) which are widely considered as mantle restites (Scott et al., 1993) formed  
67 after extraction of magmas and S-rich metallic melts. The vast majority of them are unbrecciated.  
68 They are coarse-grained peridotites consisting chiefly of olivine and pyroxenes (pigeonite, and more  
69 rarely augite and orthopyroxene), abundant carbon (< 7 wt%, graphite and diamond), with accessory  
70 metal and sulfides. Olivine grains classically have distinctive iron-depleted rims and veins (Fig. 1).  
71 They were formed by local reduction reactions with adjacent carbon. These rims give important  
72 constraints on the Ureilite Parent Body's (UPB) history. The Fe-Mg zonings of the olivines indicate  
73 that ureilites equilibrated at high temperatures (1200-1300°C), and subsequently rapidly cooled down  
74 (~2-6°C/h), consistent with impact-excavation or disruption of the UPB (e.g., Myiamoto et al., 1985).  
75 Except these rims and veins in olivine, silicates (i.e., olivine cores and pyroxenes) are quite uniform in  
76 Mg# number [= 100 Mg/(Mg+Fe), atomic] within any given ureilite. However, their compositions  
77 among samples show a huge variation, as shown by the olivine-core Mg# (= forsterite content), which  
78 range from 74 to 97. The Fe/Mn ratios (ranging from 3 to 57) and  $\Delta^{17}\text{O}$  values (= -0.2 to -2.5 ‰) are  
79 correlated with this parameter (e.g., Clayton and Mayeda, 1996; Mittlefehldt et al., 1998; Fig. 2). The  
80 origin of these variations is a matter of discussions, but no consensus emerges at present. Certainly,  
81 they cannot be explained by igneous fractionation (e.g., Mittlefehldt et al., 1998). Instead, it has been  
82 often argued that the Mg# range was ascribed to redox processes during the differentiation of the UPB  
83 or alternatively is inherited from the pre-igneous (nebular) history of the accreted materials (see  
84 Warren (2012) and Goodrich et al. (2013a) for extensive discussions of the current models on its  
85 origin).

86 A score of ureilites are polymict breccias consisting of debris of these peridotites, various  
87 chondritic clasts, and some feldspathic clasts which are remnants of the UPB's lavas (e.g., Cohen et

88 al., 2004; Downes et al., 2008). A large clast (ALM-A) has been recently discovered among the  
89 numerous stones of the Almahata Sitta fall, and demonstrate that at least part of these melts was  
90 trachyandesitic (Bischoff et al., 2014).

91 Unlike asteroids such as Vesta whose O isotopic compositions were homogenized by a magma  
92 ocean (Greenwood et al., 2005), the wide range of  $\Delta^{17}\text{O}$  values displayed by the ureilites demonstrates  
93 that the UPB was never totally melted (Clayton and Mayeda, 1996). Nevertheless, it was heated  
94 enough to generate magmas (e.g. Cohen et al., 2004; Bischoff et al., 2014) and a small S-rich core  
95 (Warren et al., 2006; Rankenburg et al., 2008; Goodrich et al., 2013b).

96 Iron isotope ratios can track the involvement of iron sulfides during the early stages of the  
97 formation of the asteroidal cores. Marked enrichments in the lighter iron isotope are found in iron  
98 sulfides formed at ca. 1000°C or below (Schuessler et al., 2007; Polyakov and Soultanov, 2011; Wang  
99 et al., 2014), whereas no iron isotope fractionation has been detected between iron sulfide, metal and  
100 silicate melts at ca. 1250°C (e.g., Hin et al., 2012). Here, we report high-precision iron isotope  
101 compositions of 30 meteorites from the UPB, and show that its mantle displays iron isotopic  
102 compositions heavier than average chondrite. This indicates that a significant fraction of the sulfides  
103 was efficiently segregated during the early stages of the melting, possibly before the melting of the  
104 silicates. Therefore, core formation in an asteroid can begin at very low degrees of partial melting  
105 through the circulation of a Fe-S melt through a silicate mantle.

106

## 107 **2. Samples and analytical procedures**

108 We analyzed 30 meteorites from the UPB (29 unbrecciated ureilites and a unique lava sample,  
109 Table 1). Samples were kindly provided by the NASA meteorite working group (MWG), the National  
110 Institute of Polar Research (NIPR), the Ecole Normale Supérieure de Lyon (ENSL), the Westfälische  
111 Wilhelms-Universität Münster, the Washington University in Saint Louis, and finally from the first  
112 author's collection. The samples from Antarctica have been extensively studied by different teams.  
113 The compositions of their phases have been repeatedly determined and their chemical features are well

114 known (the references are too numerous to be cited here). Our meteorites from Sahara have been less  
115 studied, and for most of them, only their descriptions in the Meteoritical Bulletin are available. They  
116 are all regular ureilites. We have examined polished sections of all these samples to confirm their main  
117 petrographical features, and determine the compositions of their silicates. The Saharan samples were  
118 selected in order to complement the range of compositions displayed by the Antarctic ones. Although  
119 the terrestrial weathering is pervasive in hot desert samples, the samples we selected were not severely  
120 weathered, and display partly preserved metal and sulfides.

121 The major-element compositions of the phases were determined by electron microprobe  
122 analysis using a Cameca SX100 at Service Commun de Microsonde Ouest (SCMO), Plouzané, or a  
123 JEOL JXA8200 at NIPR (Table 2). Minerals and metal standards were used for calibration. All  
124 analyses used wavelength dispersive spectrometers at 15 kV accelerating voltage, 10–30 nA beam  
125 current at NIPR, and 20 kV accelerating voltage, 40 nA beam current with the same counting time as  
126 Pierre Hudon and David Mittlefehdt (in Downes et al., 2008) at Plouzané .

127 Fragments (each of 300-1,000 mg) were crushed to a homogeneous fine powder using a boron  
128 carbide mortar and pestle. Twenty mg of crushed material was digested by sequential mixtures of  
129 HF/HNO<sub>3</sub>, HNO<sub>3</sub> and HCl for the samples analyzed in Brest and in HF/HNO<sub>3</sub> and HCl for the samples  
130 analyzed in St Louis. These procedures allow a perfect dissolution of all the phases except graphite  
131 and diamond, which are Fe-free, have no effect for our study.

132 Aliquots of the solutions were used for the determination of the Fe and Mg concentrations of  
133 in the solutions were determined by ICP-AES (inductively coupled plasma-atomic emission  
134 spectrometry) using a Horiba Jobin Yvon Ultima 2 spectrometer in Plouzané, and the Mg# numbers  
135 are given in Table 1. Iron in the dissolved samples was then purified by ion-exchange chromatography  
136 procedure previously described (Wang et al., 2012). The purification was repeated twice, thus  
137 ensuring the removal of all the matrix elements. A majority of the Fe isotopic compositions were  
138 measured on the Thermo Electron Neptune multi collector-inductively coupled plasma-mass  
139 spectrometer housed at Ifremer, Plouzané, while the rest was analyzed in Saint Louis. In both Saint  
140 Louis and Brest the instrument was operated in high resolution mode to resolve isobaric interferences,

141 such as ArO on  $^{56}\text{Fe}$ , ArOH on  $^{57}\text{Fe}$ , and ArN on  $^{54}\text{Fe}$ . We also used the sample-standard bracketing  
 142 technique to correct for instrumental mass discrimination by normalizing Fe-isotope ratios to the  
 143 average measured composition of the standard that was run before and after the sample. In Plouzané,  
 144 we performed an additional correction using Ni as an internal standard for mass bias correction  
 145 (Dauphas and Rouxel, 2006). Fe isotope values are reported relative to the standard IRMM-14 using  
 146 the  $\delta$ -notation:

$$147 \quad \delta^x\text{Fe} = 1000 \left[ \left( \frac{{}^x\text{Fe}/{}^{54}\text{Fe}}{\text{sample}} \right) / \left( \frac{{}^x\text{Fe}/{}^{54}\text{Fe}}{\text{IRMM-14}} \right) - 1 \right] \text{ where } x=56 \text{ or } 57.$$

148 Results for several georeference materials are similar to previously reported analyses (Table 3).  
 149 Errors are reported as 2 standard errors, which are calculated as the standard deviation divided by the  
 150 square root of the total number of analyses and multiplied by the Student's t-value for the relevant  
 151 degree of freedom at the 95% confidence level. Results for the samples are listed in Table 4.

152

### 153 **3. Results**

154 The  $\delta^{56}\text{Fe}$  values obtained for 30 meteorites from the UPB, fall within a restricted range, from  
 155 0.01 to 0.11‰ (Fig. 3, Table 4). The mean of all these samples is significantly heavier ( $\delta^{56}\text{Fe} = 0.056$   
 156  $\pm 0.008$  ‰,  $n=30$ ) than that of primitive meteorites, such as carbonaceous, ordinary and enstatite  
 157 chondrites ( $\delta^{56}\text{Fe} = 0.005 \pm 0.008$  ‰,  $n=42$ , Craddock et al., 2013). The heavy Fe isotope composition  
 158 displayed by the ureilites is striking because the early Solar Nebula was well homogenized for Fe  
 159 isotopes (Schoenberg and von Blanckenburg, 2006; Wang et al., 2013), and because the Fe isotope  
 160 compositions of the bulk silicate portions of most differentiated bodies investigated so far are  
 161 chondritic [e.g., the Earth (Craddock et al., 2013), Mars and Vesta (Poitrasson et al., 2004; Weyer et  
 162 al., 2005; Schoenberg and von Blanckenburg, 2006; Wang et al., 2012), and probably the Moon  
 163 (Weyer et al., 2005; Halliday et al., 2013)]. One noteworthy exception is the angrite parent body  
 164 whose lavas display high  $\delta^{56}\text{Fe}$  ratios ( $\approx 0.12$  ‰, Wang et al., 2012).

165



## 166 **4. Discussion**

### 167 **4.1. Iron inventory in ureilites**

168 Iron in ureilites is hosted by many phases: silicates (olivine and pyroxenes), metal, sulfides,  
169 phosphides, carbide (cohenite), and their weathering products (Fig. 1). It is very difficult to obtain a  
170 reliable picture of the iron budget in ureilites from modal analyses. Goodrich et al. (2014) estimated  
171 that ureilites contain ~1-3 vol.% of grain boundary metal, and less sulfides, in agreement with the  
172 abundances of metal and sulfur determined by chemistry (Vdovykin, 1970; Wänke et al., 1972;  
173 Hintenberger et al., 1978; Yanai et al., 1995). We used the standard wet chemical analyses compiled  
174 by Yanai et al. (1995) to estimate the proportions of Fe hosted by silicates, metal and troilite in  
175 ureilites (Fig. 4). Our calculations indicate that silicates are the main hosts of Fe, and represent more  
176 than 70 % of the budget of this element. Metal (14-29 % of the Fe budget) and sulfides (< 8 % of the  
177 Fe budget) are clearly subordinate hosts. These conclusions are strengthened by the striking  
178 correlation between the Mg# numbers (=100 x Mg/(Mg + Fe), atomic) of our samples and the  
179 composition of their olivine cores, which are representative of the Mg# numbers of their silicates (Fig.  
180 5).

### 181 **4.2. Origin of the high $\delta^{56}\text{Fe}$ values in ureilites**

182 The high  $\delta^{56}\text{Fe}$  values in ureilites cannot be the result of terrestrial weathering. Alteration of  
183 sulfides in meteorites is accompanied by the release of light Fe. Heavier Fe isotopic compositions have  
184 been measured in weathered ordinary chondrite finds compared to fresh falls. However, the increase is  
185 rather limited, about +0.07 ‰ of the  $\delta^{56}\text{Fe}$  were observed only for the most weathered L and H  
186 chondrites (Saunier et al., 2010). Ureilites are less prone to such an effect because sulfides control here  
187 a much lesser proportion of Fe than in L and H chondrites (Fig. 4). Although the alteration of ureilite  
188 finds is pervasive, our samples were not extensively weathered, and still displayed metal and sulfides.  
189 Indeed, the fresh fall samples (Novo Urey and Almahata Sitta) display the same isotopic compositions  
190 as find samples (Tables 1 and 4).

191           Because the Fe isotopic compositions are certainly pristine, they could be inherited from the  
192 materials which accreted to form the UPB, or alternatively they could result of the differentiation of  
193 the UPB. A heavy Fe isotopic composition could be observed in bodies that suffered evaporative loss  
194 of volatile elements following high-energy impacts during accretion. This explanation was initially  
195 proposed for the Earth and the Moon by Poitrasson et al. (2004) but is controversial for these bodies  
196 (e.g., Halliday, 2013). It is probably valid for the angrite parent body (APB), where a strong depletion  
197 in volatile elements such as the alkalis, is accompanied by heavy Fe and Si isotopic compositions  
198 (Wang et al., 2012; Pringle et al., 2014). The UPB did not accrete from volatile depleted materials,  
199 because the magmas generated by the melting of its mantle were alkali and volatile-rich as shown by  
200 the compositions of the plagioclases in the feldspathic clasts found in polymict ureilites and the  
201 geochemistry of ALM-A, a trachyandesitic lava from the UPB (e.g., Cohen et al., 2004; Bischoff et  
202 al., 2014). Nevertheless, losses of volatile elements were possible during the disruption of the UPB, as  
203 shown previously for Zn (Moynier et al., 2010). However, the lack of correlation between  $\delta^{56}\text{Fe}$  values  
204 and abundances of volatile elements (e.g., Zn, Rb, Li, not shown) rules out this possibility for Fe.

205           The high  $\delta^{56}\text{Fe}$  values in ureilites cannot be created by either the extraction of silicate melts, or  
206 by possible high temperature redox processes. Partial melting does not generate residues with  $\delta^{56}\text{Fe}$   
207 values significantly distinct than those of the initial mantle (Weyer et al., 2005; Craddock et al., 2013).  
208 High  $\delta^{56}\text{Fe}$  values in bulk rocks are certainly not the result of the reduction reactions that produced the  
209 Fe-depleted rims of the olivine during the disruption of the body. Although, the possibility of local  
210 isotopic heterogeneities in olivine have not yet been investigated, the possibility of a detectable effect  
211 is unlikely: 1/ the relative volume of the Fe-depleted rims is always limited (Fig. 1), and consequently  
212 the impact of these rims on the Fe budget is probably negligible; 2/ the formation of the Fe-depleted  
213 olivine rims was a very fast process (e.g., Myamoto et al., 1985), and a noticeable metal loss during  
214 the post-disruption cooling of the ureilites is not plausible; 3/ ALM-A, the ureilitic trachyandesite,  
215 displays a high  $\delta^{56}\text{Fe}$  value which indicates that this feature predates the disruption of the body.  
216 Moreover, the high  $\delta^{56}\text{Fe}$  values displayed by the ureilites are certainly not generated by the processes

217 that produced the striking range of olivine-core compositions. The lack of correlation between the Fe  
 218 isotope compositions of ureilites and their olivine-core compositions demonstrates that both features  
 219 are unrelated (Fig. 2).

220 Alternatively, removal of S-rich metallic melts could explain the high  $\delta^{56}\text{Fe}$  values in ureilites.  
 221 When a chondritic assemblage is heated, melting begins with Fe-sulfide (troilite) and metal at a  
 222 temperature close to 980°C defined by the eutectic in the Fe-FeS system (Keil, 2000). Since at this  
 223 temperature FeS displays a marked enrichment in the lighter Fe isotope (Schuessler et al., 2007,  
 224 Polyakov and Soultanov, 2011; Wang et al., 2014), an increase of the  $\delta^{56}\text{Fe}$  value of the solid residue  
 225 is anticipated. If the metallic melt is efficiently removed from the solid residue (fractional melting), all  
 226 melting happens at the eutectic until either metal or troilite is exhausted. The effect on the isotopic  
 227 compositions of the residues can be easily estimated.

228 The eutectic in the Fe-FeS system contains about 31.6 wt% S and 68.4 wt% Fe (e.g., Kullerud,  
 229 1963), and is equivalent to about 85 wt% troilite +15 wt% metal. We calculate the  $\Delta^{56}\text{Fe}_{\text{metallic melt-silicate}}$   
 230 using these proportions, the  $\Delta^{56}\text{Fe}_{\text{troilite-silicate}}$  value (-0.21 ‰) selected by Wang et al. (2014) and the  
 231  $\Delta^{56}\text{Fe}_{\text{metal-troilite}}$  at ca. 1250 K (+0.1 - +0.2 ‰) estimated from theoretical calculations (Polyakov et al.,  
 232 2007; Polyakov and Soultanov, 2011). For the calculations presented in Figure 6, we used a  
 233  $\Delta^{56}\text{Fe}_{\text{metallic melt-silicate}} = -0.18$  ‰, and assumed that  $\Delta^{56}\text{Fe}_{\text{metallic melt-silicate}} \approx \Delta^{56}\text{Fe}_{\text{metallic melt-residue}}$ .

234 The composition of a source after extraction of a S-rich metallic melt at the eutectic were  
 235 calculated using an isotope mass balance:

$$236 \quad \delta^{56}\text{Fe}_{\text{source}} = \delta^{56}\text{Fe}_{\text{metallic melt}} \cdot f_{\text{Fe}_{\text{metallic melt}}} + \delta^{56}\text{Fe}_{\text{residue}} \cdot f_{\text{Fe}_{\text{residue}}} \quad (1)$$

237 where  $f$  is the mass fraction of  $^{54}\text{Fe}$  in the metallic melt or in the solid residue. This equation  
 238 can be recast in terms of the residue:

$$239 \quad \delta^{56}\text{Fe}_{\text{source}} = (\Delta^{56}\text{Fe}_{\text{metallic melt-residue}} + \delta^{56}\text{Fe}_{\text{residue}}) (1 - f_{\text{Fe}_{\text{residue}}}) + \delta^{56}\text{Fe}_{\text{residue}} \cdot f_{\text{Fe}_{\text{residue}}} \quad (2)$$

240 And consequently:

241 
$$\delta^{56}\text{Fe}_{\text{residue}} = \delta^{56}\text{Fe}_{\text{source}} - \Delta^{56}\text{Fe}_{\text{metallic melt-residue}} + \Delta^{56}\text{Fe}_{\text{metallic melt-residue}} \cdot f_{\text{Fe}_{\text{residue}}} \quad (3)$$

242 Calculations show that detectable shift of the Fe isotopic compositions is possible, depending  
 243 on the initial Fe and S contents of the starting assemblage (Fig. 6). If the starting assemblage is Fe-rich  
 244 and displays moderate S contents (e.g., like a H chondrite), segregation of the metallic melt produces  
 245 at best a marginal shift of the isotopic composition of the residue. In contrast, for S-rich chondritic  
 246 assemblages, an increase of ca. 0.1 ‰ of the  $\delta^{56}\text{Fe}$  can be achieved by this process.

247 If the metallic melt is not removed from the residue (batch melting), the degree of melting  
 248 increases with the temperature. The composition of the metallic melt is consequently variable, and the  
 249 situation becomes much more complex (melting of the silicates, involvement of carbon...). More  
 250 importantly, fractionation of Fe isotopes between S-rich metallic melts and silicates becomes much  
 251 less detectable with increasing temperature, and is usually supposed negligible considering our present  
 252 level of precision, above 1250°C as determined through experimental studies (Poitrasson et al., 2009;  
 253 Hin et al., 2012). [Notice that this view has been recently challenged by Shahar et al. (2015) whose  
 254 results indicate significant fractionations between metallic melts and melted silicates at 1600°C.  
 255 However, the magnitude and direction of these isotopic fractionations are not consistent with the  
 256 available analyses on magmatic irons (bulk samples) and the results presented here. A discussion of  
 257 these results and previous ones is beyond the scope of this paper. Additional works are necessary to  
 258 confirm these experimental results and to evaluate the effects of B or Sn used in previous  
 259 experiments.]

260 Siderophile element systematics (e.g. platinum group elements) demonstrate that ureilites  
 261 experienced separation of S-rich metallic melts, with possibly entrainment of metal (Warren et al.,  
 262 2006; Rankenburg et al., 2008; Goodrich et al., 2013b), but the process (batch or fractional) and  
 263 temperatures of segregation are not well constrained by these data. The heavy Fe isotopic  
 264 compositions and the low S contents of the ureilites are consistent with the separation of S-rich  
 265 metallic melts (Fig. 6), and indicate that the removal of these melts was efficient probably at a  
 266 temperature close to the eutectic, and certainly before the onset of the melting of the silicates (< 1100

267 °C). Indeed, ALM-A, the sole ureilitic lava sample available at present (Bischoff et al., 2014), displays  
 268 a high  $\delta^{56}\text{Fe}$  value (Fig. 3), similar to the highest values measured on ureilites. Although partial  
 269 melting can generate melts with Fe isotopic compositions heavier than their sources as exemplified by  
 270 terrestrial basalts (e.g., Teng et al., 2013), this effect is negligible for mantles with low  $\text{Fe}^{3+}/\text{Fe}_{\text{total}}$   
 271 ratios (Dauphas et al., 2014), like ureilites (Goodrich et al., 2013c). Consequently, ALM-A strongly  
 272 suggests that the UPB's mantle acquired its specific isotopic composition early, before it was heated  
 273 enough to generate magmas.

#### 274 **4.3. Comparison with mantles of other small bodies.**

275 The heavy Fe isotopic compositions displayed by ureilites contrast with those of the  
 276 brachinites and the olivines from the Main Group Pallasites, the samples of the other asteroidal  
 277 mantles for which data are available (Fig. 3). Brachinites were possibly derived from multiple parent  
 278 bodies. They are mantle restites similar to ureilites, but are more ferroan than the latter (Keil, 2014).  
 279 GRA 06128/29, a brachinitic melt shows a light Fe isotopic composition ( $\delta^{56}\text{Fe} = -0.08 \pm 0.06 \text{ ‰}$ ),  
 280 which was ascribed to the involvement of Fe-sulfides during magma genesis (Wang et al., 2014).  
 281 Probably because of the high Fe content of their protoliths, the average composition of the brachinites  
 282 does not deviate from the chondritic value ( $\delta^{56}\text{Fe} = 0.01 \pm 0.02 \text{ ‰}$ ,  $n=7$ , Wang et al., 2014), although  
 283 S-rich metallic melts and sulfides were certainly involved during their differentiation (Day et al.,  
 284 2012). Main Group Pallasites (MGPs) are mixtures of mantle-derived olivines and core-derived metal  
 285 from a single disrupted asteroid (Greenwood et al., 2006). The homogeneous O isotopic composition  
 286 of these pallasites provides a strong evidence for an early extensive melting event on their parent  
 287 body, possibly resulting in the formation of a global magma ocean (Greenwood et al., 2006). Fe  
 288 isotopes in MGPs cannot record the early stages of core segregation, because the temperatures reached  
 289 during the global melting event were too high ( $\gg 1300^\circ\text{C}$ ) to fractionate these isotopes between  
 290 silicates and metallic melts. Indeed, the average Fe isotopic composition of olivines ( $\delta^{56}\text{Fe} = 0.009 \pm$   
 291  $0.014 \text{ ‰}$ ,  $n=11$ , Weyer et al., 2005) is indistinguishable from the chondritic average.

292

## 293 5. Conclusions

294 The marked S depletions, the siderophile element abundances and the high  $\delta^{56}\text{Fe}$  values  
295 displayed by ureilites point to an efficient segregation of S-rich metallic melts in the body, more likely  
296 before the onset of silicate melting. Although the UPB has been disrupted, samples of its core have not  
297 yet been recovered. The lack of such samples is not surprising because the number of meteorites from  
298 the UPB is still limited. The fact that only one large clast of ureilitic lava is actually known  
299 demonstrates that our ureilite meteorites provide only a partial sampling of the whole parent body.

300 The percolation of S-rich metallic melts has been extensively investigated in a solid matrix  
301 rich in olivine, analogous to an asteroidal mantle. Metallic melts over a percolation threshold ranging  
302 from about 6 vol% to 18 vol% (Yoshino et al., 2003; Bagdassarov et al., 2009; Watson and Roberts,  
303 2011) can potentially create a stable interconnected network in an olivine-rich solid matrix that could  
304 have allowed the early segregation of some core material. Yet the permeability of the core forming Fe-  
305 FeS melts within a silicate matrix is very low, and it was inferred that percolation of these melts  
306 cannot be a major process of core formation in planetesimals (Watson and Roberts, 2011). The  
307 geochemical data on ureilites seem at odds with previous experiments. Certainly other factors can  
308 contribute to the segregation of Fe-FeS melts and to fast core formation in planetesimals, such as shear  
309 deformation of the body (Bruhn et al., 2000; Rushmer and Petford, 2011).

310

### 311 **Acknowledgements:**

312 Many samples analyzed during the course of this study were kindly provided by the National  
313 Institute of Polar Research and the NASA meteorite working group. US Antarctic meteorite samples  
314 are recovered by the Antarctic search for Meteorites (ANSMET) program which has been funded by  
315 NSF and NASA, and characterized and curated in the department of Mineral Sciences of the  
316 Smithsonian Institution and Astromaterials Curation Office at NASA Johnson Space Center. We thank  
317 Bernard Marty for the editorial handling, Hilary Downes, Franck Poitrasson, and an anonymous  
318 reviewer for their fast and constructive comments, Albert Jambon, Mathieu Roskosz and Richard  
319 Greenwood for discussions, and Pascale Barrat for her help. We gratefully acknowledge the  
320 Programme National de Planétologie (CNRS-INSU) for financial support.

## References

- 321  
322  
323 Bagdassarov, N., Golabek, G.J., Solferino, G., Schmidt, M.W. (2009) Constraints on the Fe–S melt connectivity in mantle  
324 silicates from electrical impedance measurements. *Phys. Earth Planet. Inter.* **177**, 139–146.  
325  
326 Bischoff, A. et al. (2014) Trachyandesitic magmatism in the early Solar System. *Proc. Natl. Acad. Sci. USA* **111**, 35, 12689-  
327 12692.  
328  
329 Blichert-Toft J., Moynier F., Lee C.T.A., Telouk P., Albarede F. (2010) The early formation of the IVA iron meteorite parent  
330 body. *Earth Planet. Sci. Lett.* **296**, 469-480.  
331  
332 Bruhn, D., Groebner, N., Kohlstedt, D.L. (2000) An interconnected network of core-forming melts produced by shear  
333 deformation. *Nature* **403**, 883-886.  
334  
335 Cohen, B.A., Goodrich, C.A., Keil, K. (2004) Feldspathic clast populations in polymict ureilites: Stalking the missing basalts  
336 from the ureilite parent body. *Geochim. Cosmochim. Acta* **68**, 4249–4266.  
337  
338 Clayton R.N., Mayeda T.K. (1996) Oxygen isotope studies of achondrites. *Geochim. Cosmochim. Acta* **60**, 1999-2017.  
339  
340 Craddock, P.R., Dauphas, N. (2011) Iron isotopic compositions of geological reference materials and chondrites. *Geostand.*  
341 *Geoanal. Res.* **35**, 101–123.
- 342 Craddock, P.R., Warren, J.M., Dauphas, N. (2013) Abyssal peridotites reveal the near-chondritic Fe isotopic composition of  
343 the Earth. *Earth Planet. Sci. Lett.* **365**, 63–76.
- 344 Dauphas N. et al. (2014) Magma redox and structural controls on iron isotope variations in the Earth’s mantle and crust.  
345 *Earth Planet. Sci. Lett.* **398**, 127-140.  
346  
347 Dauphas, N., Rouxel, O. (2006) Mass spectrometry and natural variations of iron isotopes. *Mass Spectrometry Reviews* **25**,  
348 515-550.  
349  
350 Day, J.M.D. et al. (2012) Origin of felsic achondrites Graves Nunataks 06128 and 06129, and ultramafic brachinites and  
351 brachinite-like achondrites by partial melting of volatile-rich primitive parent bodies. *Geochim. Cosmochim. Acta* **81**, 94–  
352 128.  
353  
354 Downes, H., Mittlefehldt, D.W., Kita, N.T., Valley, J.W. (2008) Evidence from polymict ureilite meteorites for a disrupted  
355 and re-accreted single ureilite parent asteroid gardened by several distinct impactors. *Geochim Cosmochim Acta* **72**, 4825–  
356 4844.  
357  
358 Goodrich, C. A., Wlotzka, F., Ross, D. K. and Bartoschewitz, R. (2006) NWA 1500: plagioclase-bearing monomict ureilite  
359 or ungrouped achondrite? *Meteorit. Planet. Sci.* **41**, 925–952.  
360  
361 Goodrich C.A., Wilson L., van Orman J.A., Michel P. (2013a) Comment on “Parent body depth-pressure-temperature  
362 relationships and the style of the ureilite anatexis” by P. H. Warren (MAPS 47:209–227) *Meteoritics & Planetary Science* **48**  
363 1096-1106.  
364  
365 Goodrich, C. A., Ash, R. D., Van Orman, J. A., Domanik, K., McDonough, W. F. (2013b) Metallic phases and siderophile  
366 elements in main group ureilites: implications for ureilite petrogenesis. *Geochim. Cosmochim. Acta* **112**, 340–373.  
367  
368 Goodrich C.A., Sutton S.R., Wirick S., Jercinovic M.J. (2013c) Chromium valences in ureilite olivine and implications for  
369 ureilite petrogenesis. *Geochim. Cosmochim. Acta* **122**, 280-305.  
370  
371 Goodrich C.A., Harlow G.E., Van Orman J.A., Sutton S.R., Jercinovic M.J., Mikouchi T. (2014) Petrology of chromite in  
372 ureilites: Deconvolution of primary oxidation states and secondary reduction processes. *Geochim. Cosmochim. Acta* **135**,  
373 126-169.  
374  
375 Greenwood, R.C., Franchi, I.A., Jambon, A., Buchanan, P. (2005) Widespread magma oceans on asteroidal bodies in the  
376 early solar system. *Nature* **435**, 916-918.  
377  
378 Greenwood, R.C., Franchi, I.A., Jambon, A., Barrat, J.A., Burbine, T.H. (2006) Oxygen isotope variation in stony-iron  
379 meteorites. *Science* **313**, 1763-1765.  
380  
381 Halliday, A.N. (2013) Small differences in sameness. *Nature* **497**, 43-45.  
382

- 383 Hin, R.C., Schmidt, M.W., Bourdon, B. (2012) Experimental evidence for the absence of iron isotope fractionation between  
384 metal and silicate liquids at 1 GPa and 1250-1300°C and its cosmochemical consequences. *Geochim. Cosmochim. Acta* **93**,  
385 164-181.
- 386  
387 Hintenberger H., Jochum K.P., Braun O., Christ P., Martin W. (1978) The antarctic meteorite Yamato 74123 – a new ureilite.  
388 *Earth Planet. Sci. Lett.* **40**, 187-193.
- 389  
390 Keil, K. (2000) Thermal alteration of asteroids: evidence from meteorites. *Planet. Space Sci.* **48**, 887-903.
- 391  
392 Keil, K. (2014) Brachinite meteorites: Partial melt residues from an FeO-rich asteroid. *Chemie der Erde* **74**, 311-329.
- 393  
394 Kruijer, T.S. et al. (2014) Protracted core formation and rapid accretion of protoplanets. *Science* **344**, 1150-1154.
- 395  
396 Kullerud G. (1963) The Fe-Ni-S system. *Ann. Rep. Geophys. Lab.* **67**, 4055-4061.
- 397  
398 Mittlefehldt, D.W., McCoy, T.J., Goodrich, C.A., Kracher, A., (1998) Non-chondritic meteorites from asteroidal bodies. In:  
399 Papike, J.J.(Ed.), Planetary Materials. Mineralogical Society of America, Washington, DC, p.195.
- 400  
401 Moynier F, Beck P., Yin Q.Z., Ferroir T., Barrat J.A., Paniello R., Telouk P., Gillet P. (2010) Volatilization induced by  
402 impacts recorded in Zn isotope composition of ureilites. *Chem. Geol.* **276**, 374-379.
- 403  
404 Myiamoto M., Takeda H., Toyoda H. (1985) Cooling history of some Antarctic ureilites. *J Geophys. Res.* **90**, supplement,  
D116-D122.
- 405  
406 Poitrasson, F., Halliday, A.N., Lee, D.C., Levasseur, S., Teutsch, N. (2004) Iron isotope differences between Earth, Moon,  
Mars and Vesta as possible records of contrasted accretion mechanisms. *Earth Planet. Sci. Lett.* **223**, 253–266.
- 407  
408 Poitrasson, F., Roskosz, M. and Corgne, A. (2009) No iron isotope fractionation between molten alloys and silicate melt to  
409 2000 degrees C and 7.7 GPa: experimental evidence and implications for planetary differentiation and accretion. *Earth*  
410 *Planet. Sci. Lett.* **278**, 376–385.
- 411  
412 Polyakov, V. B., Clayton, R. N., Horita, J. and Mineev, S. D. Equilibrium iron isotope fractionation factors of minerals:  
413 reevaluation from the data of nuclear inelastic resonant X-ray scattering and Mössbauer spectroscopy. *Geochim. Cosmochim.*  
414 *Acta* **71**, 3833–3846 (2007).
- 415  
416 Polyakov, V. B. and Soultanov, D. M (2011) New data on equilibrium iron isotope fractionation among sulfides: constraints  
417 on mechanisms of sulfide formation in hydrothermal and igneous systems. *Geochim. Cosmochim. Acta* **75**, 1957–1974.
- 418  
419 Pringle E.A., Moynier F., Savage P.S., Badro J., Barrat J.A. (2014) Silicon isotopes in angrites and volatile loss in  
420 planetesimals. *Proc. Natl. Acad. Sci. USA*, doi: 10.1073/pnas.1418889111.
- 421  
422 Rankenburg, K., Humayun, M., Brandon, A. D., Herrin, J. S. (2008) Highly siderophile elements in ureilites. *Geochim.*  
423 *Cosmochim. Acta* **72**, 4642–4659.
- 424  
425 Rushmer T., Petford N. (2011) Microsegregation rates of liquid Fe-Ni-S metal in natural silicate-metal systems: A combined  
426 experimental and numerical study. *Geochim Geophys. Geosyst.* **12**, Q03014, doi: 10.1029/2010GC003413.
- 427  
428 Saunier G., Poitrasson F., Moine B., Gregoire M., Seddiki A. (2010) Effect of hot desert weathering on the bulk-rock iron  
429 isotope composition of L6 and H5 ordinary chondrites. *Meteorit. Planet. Sci.* **45**, 195-209.
- 430  
431 Schoenberg, R., von Blanckenburg, F. (2006) Modes of planetary-scale Fe isotope fractionation. *Earth Planet. Sci. Lett.* **252**,  
432 342–359.
- 433  
434 Schuessler, J.A., Schoenberg, R., Behrens, H., von Blanckenburg, F. (2007) The experimental calibration of the iron isotope  
435 fractionation factor between pyrrhotite and peralkaline rhyolitic melt. *Geochim. Cosmochim. Acta* **71**, 417-433.
- 436  
437 Scott, E.R.D., Taylor, G.J., Keil, K. (1993) Origin of ureilite meteorites and implications for planetary accretion. *Geophys.*  
438 *Res. Lett.* **20**, 415–418.
- 439  
440 Shahar, A. et al. (2015) Sulfur-controlled iron isotope fractionation experiments of core formation in planetary bodies.  
441 *Geochim. Cosmochim. Acta* **150**, 253-264.
- 442  
443 Singletary, S. J. and Grove, T. L. (2003) Early petrologic processes on the ureilite parent body. *Meteorit. Planet. Sci.* **38**, 95–  
444 108.
- 445  
446 Teng F.Z., Dauphas N., Huang S., Marty B. (2013) Iron isotopic systematics of oceanic basalts. *Geochim. Cosmochim. Acta*  
**107**, 12-26.



- 447  
448 Vdovykin G. P. (1970) Ureilites. *Space Sci. Rev.* **10**, 483–510.  
449
- 450 Wang, K. *et al.* (2012) Iron isotope fractionation in planetary crusts. *Geochim. Cosmochim. Acta* **89**, 31–45.  
451
- 452 Wang, K. *et al.* (2013) Homogeneous distribution of Fe isotopes in the early solar nebula. *Meteorit. Planet. Sci.* **48**, 354–364.  
453
- 454 Wang, K. *et al.* (2014) Iron isotope fractionation during sulfide-rich felsic partial melting in early planetesimals. *Earth Planet. Sci. Lett.* **392**, 124–132.  
455
- 456 Wänke H., Baddenhausen H., Spettel B., Teschke F., Quijano-Rico M., Dreibus G., Palme H. (1972) The chemistry of , 572-  
457 590Haverö ureilite. *Meteoritics* **7**, 579-590.  
458
- 459 Warren P.H. (2011) Stable isotopes and the noncarbonaceous derivation of ureilites, in common with nearly all differentiated  
460 planetary materials. *Geochim. Cosmochim. Acta* **75**, 6912-6926.  
461
- 462 Warren P. H. (2012) Parent body depth-pressure-temperature relationships and the style of the ureilite anatexis. *Meteoritics  
& Planetary Science* **47**, 209–227.  
463
- 464 Warren, P. H. and Rubin, A. E. (2010) Pyroxene-selective impact smelting in ureilites. *Geochim. Cosmochim. Acta* **74**, 5109–  
465 5133.  
466
- 467 Warren, P.H., Ulff-Moller, F., Huber, H., Kallemeyn, G.W. (2006) Siderophile geochemistry of ureilite: a record of early  
468 stages of planetesimal core formation. *Geochim. Cosmochim. Acta* **70**, 2104-2126.  
469
- 470 Wasson, J.T., Kallemeyn, G.W. (1988) Compositions of chondrites. *Phil. Trans. R. Soc. London A* **325**, 535-544.  
471
- 472 Watson, H.C., Roberts, J.J. (2011) Connectivity of core forming melts: Experimental constraints from electrical conductivity  
473 and X-ray tomography. *Phys. Earth Planet. Inter.* **186**, 172-182.  
474
- 475 Weyer, S. *et al.* (2005) Iron isotope fractionation during planetary differentiation. *Earth Planet. Sci. Lett.* **240**, 251–264.  
476
- 477 Yanai K., Kojma H., Haramura H. (1995) Catalog of the Antarctic meteorites. National Institute of Polar Research, Tokyo,  
478 230 p.  
479
- 480 Yoshino, T., Walter, M.J., Katsura, T. (2003) Core formation in planetesimals triggered by permeable flow. *Nature* **422**, 154–  
481 157.  
482  
483

484 Table 1. Details of meteorite samples studied. Olivine compositions are from this study except D  
 485 (Downes et al., 2008), SG (Singletary and Grove, 2004), G (Goodrich et al., 2006), and WR (Warren  
 486 and Rubin, 2010).

	Source	# or split	Olivine core Fo %	bulk rock Mg#
<b><i>Fall</i></b>				
Novo Urei	Saint Louis		78.5 <sup>SG</sup>	
<b><i>Hot desert finds</i></b>				
El Gouanem	ENS Lyon		80.7 <sup>SG</sup>	
NWA 2236	NIPR	,41	96.8	91.8
NWA 4471	JAB		78.1	70.2
NWA 4509	ENS Lyon		78.5	
NWA 4511	ENS Lyon		77.8	77.2
NWA 4512	ENS Lyon		78.3	
NWA 4513	ENS Lyon		90.5	
NWA 4516	ENS Lyon		81.3	76.9
NWA 5555	JAB		90.8	87.3
NWA 5602	JAB		79.0	76.5
NWA 5884	JAB		78.6	75.0
NWA 6056	JAB		84.8	81.4
NWA 7349	JAB		76.5	75.4
NWA 7630	JAB		79.1	73.4
NWA 7686	JAB		91.0	84.3
NWA 7880	JAB		78.6	77.7
NWA 8049	JAB		84.3	81.3
<b><i>Antarctic finds</i></b>				
A-881931	NIPR	,65	78.7	76.5
ALHA 77257	NIPR	,104	86.1 <sup>D</sup>	83.7
ALH 82130	MWG	,43	95.2 <sup>D</sup>	89.9
EET 83225	MWG	,37	88.3 <sup>D</sup>	85.5
LAP 03587	MWG	,10	74.7 <sup>WR</sup>	74.1
LAR 04315	MWG	,46	81.9 <sup>WR</sup>	79.1
MET 01085	MWG	,23	no olivine	84.9
Y-791538	NIPR	,126	91.3 <sup>D</sup>	87.1
Y-981810	NIPR	,88	78.3	74.4
<b><i>Other finds</i></b>				
Kenna	Saint Louis		78.0 <sup>G</sup>	
Goalpara	Saint Louis		76.6 <sup>D</sup>	
<b><i>Ureilitic trachyandesite (Almahata Sitta fall)</i></b>				
ALM-A	Münster		no olivine	

488 Table 2. Olivine core compositions of the samples analyzed during the course of this study (oxides in  
 489 wt%, Fe/Mn atomic).

490

	lab.	n	SiO <sub>2</sub>	Cr <sub>2</sub> O <sub>3</sub>	FeO	MnO	MgO	CaO	total	Fo%	Fe/Mn
A-881931	NIPR	13	38.07	0.49	19.72	0.40	40.78	0.29	99.75	78.7	48.1
NWA2236	NIPR	28	42.38	0.38	3.21	0.45	53.91	0.28	100.64	96.8	7.0
NWA 4471	SCMO	10	38.75	0.49	19.92	0.39	39.92	0.29	99.76	78.1	50.1
NWA 4509	SCMO	10	39.06	0.75	19.73	0.41	40.49	0.37	100.80	78.5	48.0
NWA 4511	SCMO	10	38.80	0.54	20.32	0.40	40.03	0.31	100.40	77.8	50.7
NWA 4512	SCMO	10	39.47	0.71	19.75	0.40	39.95	0.37	100.67	78.3	48.2
NWA 4513	SCMO	10	40.82	0.59	9.08	0.43	48.52	0.30	99.74	90.5	20.8
NWA 4516	SCMO	10	39.19	0.67	17.38	0.41	42.28	0.32	100.26	81.3	41.5
NWA5555	SCMO	10	41.07	0.62	8.89	0.45	49.36	0.31	100.72	90.8	19.5
NWA 5602	SCMO	10	38.60	0.72	19.32	0.41	40.88	0.35	100.28	79.0	46.3
NWA5884	SCMO	10	39.32	0.70	19.36	0.40	39.92	0.32	100.06	78.6	47.4
NWA6056	SCMO	10	40.26	0.75	14.27	0.44	44.73	0.39	100.87	84.8	31.8
NWA 7349	SCMO	10	38.54	0.39	21.55	0.41	39.29	0.23	100.41	76.5	51.3
NWA 7630	SCMO	10	38.89	0.74	19.26	0.41	40.78	0.33	100.40	79.1	46.6
NWA 7686	SCMO	10	40.88	0.64	8.65	0.45	49.16	0.34	100.15	91.0	19.1
NWA 7880	SCMO	10	38.82	0.74	19.69	0.40	40.58	0.28	100.54	78.6	49.2
NWA 8049	SCMO	10	39.85	0.71	14.66	0.42	44.11	0.37	100.11	84.3	34.5
Y-981810	NIPR	18	38.64	0.55	20.05	0.39	40.54	0.35	100.51	78.3	50.2

491

492

493

494 Table 3. Iron isotopic compositions of international standards obtained during the course of this study  
 495 in Saint Louis and in Plouzané, and compared with literature values. (N# = number of runs of the same  
 496 solution).

	N#	$\delta^{56}\text{Fe}$	95% C.I.	$\delta^{57}\text{Fe}$	95% C.I.
<b>BIR1</b>					
Plouzané, average (n=6)		<b>0.073</b>	<b>±0.017</b>	<b>0.116</b>	<b>±0.013</b>
Wang et al. (2012)		0.043	±0.016	0.058	±0.026
Craddock & Dauphas (2011)		0.053	±0.015	0.087	±0.023
<b>BHVO2</b>					
Plouzané, average (n=14)		<b>0.117</b>	<b>±0.011</b>	<b>0.181</b>	<b>±0.023</b>
Wang et al. (2012)		0.102	±0.012	0.159	±0.018
Craddock & Dauphas (2011)		0.114	±0.011	0.174	±0.016
<b>Allende USNM3529</b>					
Plouzané #1	5	0.015	±0.015	0.014	±0.069
Plouzané #2	5	0.021	±0.035	-0.019	±0.039
Plouzané, average (n=2)		<b>0.018</b>		<b>-0.003</b>	
Craddock & Dauphas (2011)		-0.007	±0.012	0.003	±0.019
<b>AC-E</b>					
Plouzané #1	5	0.316	±0.025	0.501	±0.065
Wang et al. (2012)		0.313	±0.018	0.457	±0.028
Craddock & Dauphas (2011)		0.320	±0.010	0.478	±0.015

497

498

499

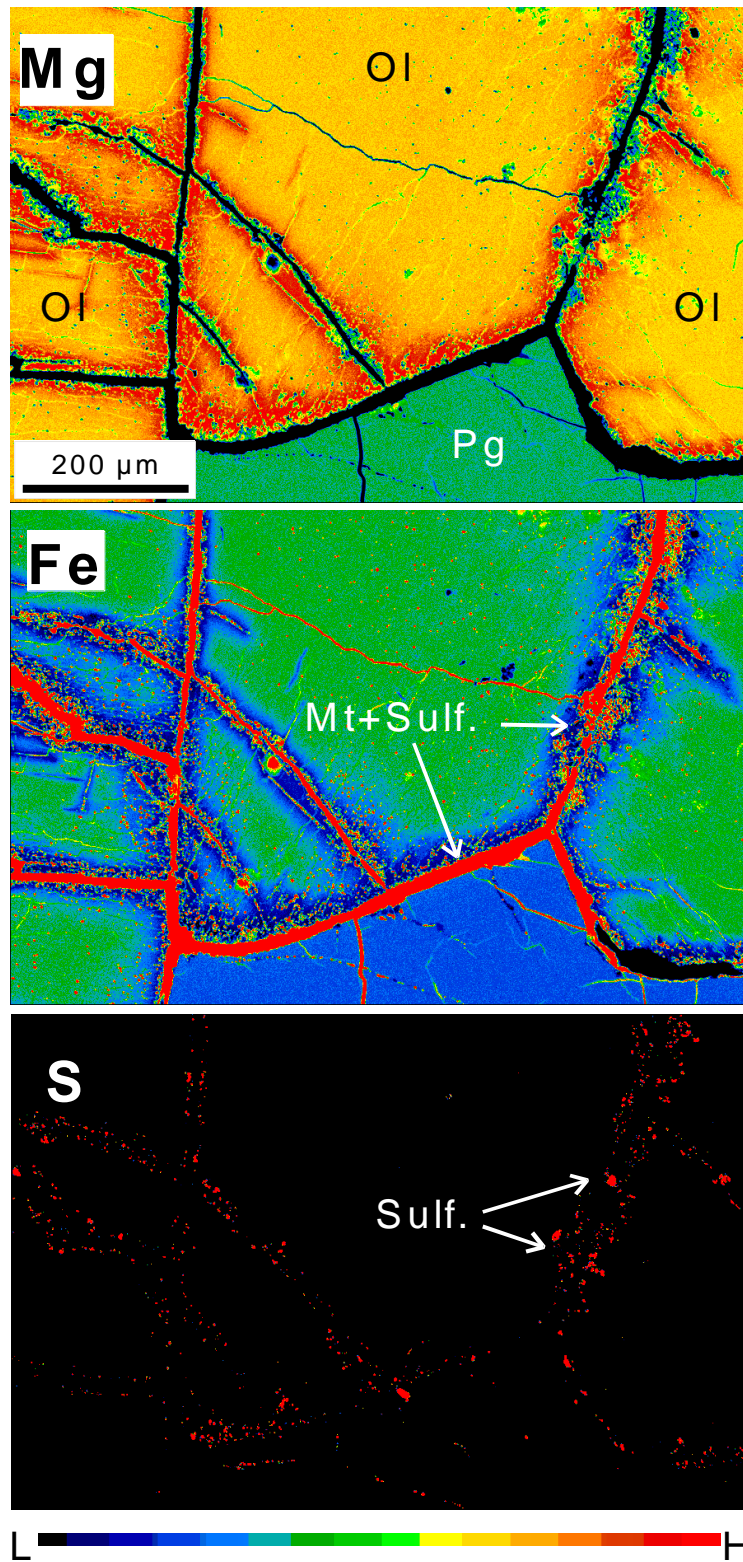
500 Table 4. Iron isotopic compositions of unbrecciated and trachyandesitic ureilites.

	lab.	N#	$\delta^{56}\text{Fe}$	95% C.I.	$\delta^{57}\text{Fe}$	95% C.I.	
<b><i>Fall</i></b>							
	Novo Urei #1	St Louis	9	0.024	$\pm 0.030$	0.027	$\pm 0.050$
	Novo Urei #2	St Louis	9	0.039	$\pm 0.038$	0.084	$\pm 0.057$
<b><i>Northwest Africa finds</i></b>							
	El Gouanem	St Louis	9	0.068	$\pm 0.028$	0.085	$\pm 0.052$
	NWA 2236	Plouzané	6	0.076	$\pm 0.017$	0.129	$\pm 0.047$
	NWA 4471	Plouzané	8	0.086	$\pm 0.021$	0.133	$\pm 0.033$
	NWA 4509	St Louis	9	0.024	$\pm 0.033$	0.060	$\pm 0.058$
	NWA 4511 #1	Plouzané	8	0.051	$\pm 0.032$	0.073	$\pm 0.052$
	NWA 4511 #2	St Louis	8	0.023	$\pm 0.032$	0.062	$\pm 0.059$
	NWA 4512	St Louis	8	0.046	$\pm 0.032$	0.082	$\pm 0.059$
	NWA 4513	St Louis	9	0.054	$\pm 0.038$	0.098	$\pm 0.057$
	NWA 4516	Plouzané	9	0.047	$\pm 0.030$	0.073	$\pm 0.044$
	NWA 5555	Plouzané	7	0.053	$\pm 0.031$	0.081	$\pm 0.047$
	NWA 5602	Plouzané	10	0.043	$\pm 0.029$	0.065	$\pm 0.049$
	NWA 5884	Plouzané	7	0.057	$\pm 0.017$	0.087	$\pm 0.028$
	NWA 6056 #1	Plouzané	5	0.040	$\pm 0.025$	0.027	$\pm 0.027$
	NWA 6056 #2	Plouzané	7	0.054	$\pm 0.021$	0.080	$\pm 0.035$
	NWA 7349	Plouzané	8	0.059	$\pm 0.018$	0.094	$\pm 0.027$
	NWA 7630	Plouzané	7	0.081	$\pm 0.026$	0.124	$\pm 0.037$
	NWA 7686 #1	Plouzané	5	0.090	$\pm 0.017$	0.117	$\pm 0.066$
	NWA 7686 #2	Plouzané	7	0.067	$\pm 0.029$	0.103	$\pm 0.047$
	NWA 7880	Plouzané	6	0.040	$\pm 0.022$	0.063	$\pm 0.030$
	NWA 8049	Plouzané	7	0.067	$\pm 0.031$	0.109	$\pm 0.055$
<b><i>Antarctic finds</i></b>							
	A-881931	Plouzané	5	0.109	$\pm 0.039$	0.209	$\pm 0.062$
	ALHA 77257	Plouzané	6	0.058	$\pm 0.030$	0.079	$\pm 0.057$
	ALH 82130	Plouzané	8	0.044	$\pm 0.034$	0.053	$\pm 0.045$
	EET 83225	Plouzané	6	0.035	$\pm 0.026$	0.038	$\pm 0.067$
	LAP 03587 #1	Plouzané	7	0.035	$\pm 0.030$	0.075	$\pm 0.016$
	LAP 03587 #2	St Louis	9	0.055	$\pm 0.033$	0.082	$\pm 0.058$
	LAR 04315	Plouzané	6	0.059	$\pm 0.029$	0.088	$\pm 0.057$
	MET 01085	Plouzané	6	0.023	$\pm 0.023$	0.036	$\pm 0.055$
	Y-791538	Plouzané	6	0.071	$\pm 0.018$	0.121	$\pm 0.045$
	Y-981810	Plouzané	5	0.077	$\pm 0.015$	0.125	$\pm 0.073$
<b><i>Other finds</i></b>							
	Kenna	St Louis	9	0.009	$\pm 0.030$	0.030	$\pm 0.049$
	Goalpara #1	St Louis	9	0.048	$\pm 0.030$	0.095	$\pm 0.049$
	Goalpara #2	St Louis	9	0.056	$\pm 0.038$	0.092	$\pm 0.057$
<b><i>Ureilitic trachyandesite</i></b>							
	ALM-A #1	Plouzané	5	0.095	$\pm 0.032$	0.155	$\pm 0.066$
	ALM-A #2	Plouzané	4	0.096	$\pm 0.019$	0.107	$\pm 0.045$
	ALM-A #3	Plouzané	8	0.105	$\pm 0.023$	0.159	$\pm 0.038$

501

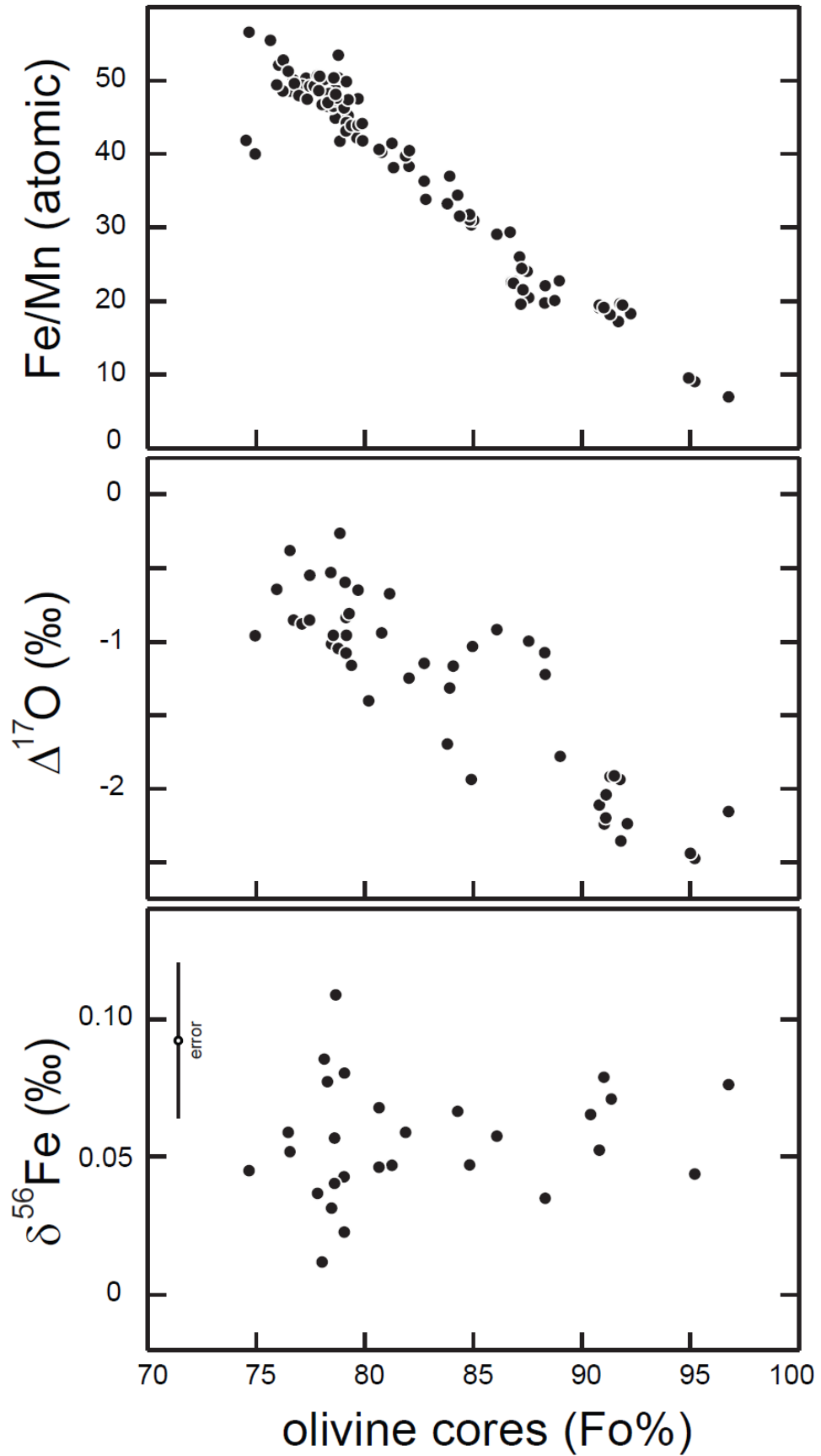
502

503



504  
 505  
 506  
 507  
 508  
 509  
 510

Figure 1. Maps of Mg, Fe and S of Northwest Africa 8049, a typical ureilite, showing the zoning of the olivine grains (Ol), the homogeneity of the pigeonite (Pg), and the repartition of metal (Mt - mainly interstitial and in tiny inclusions into olivine) and sulfides (Sulf.).



511  
 512  
 513  
 514  
 515

Figure 2. Plots of molar Fe/Mn ratios in olivine cores,  $\Delta^{17}\text{O}$  (Clayton and Mayeda, 1996) and  $\delta^{56}\text{Fe}$  in the bulk rocks vs. the composition of the olivine cores (data from Table 2, and mainly from Downes et al. (2008), Singletary and Grove (2003), Goodrich et al. (2006, 2014) and references therein).

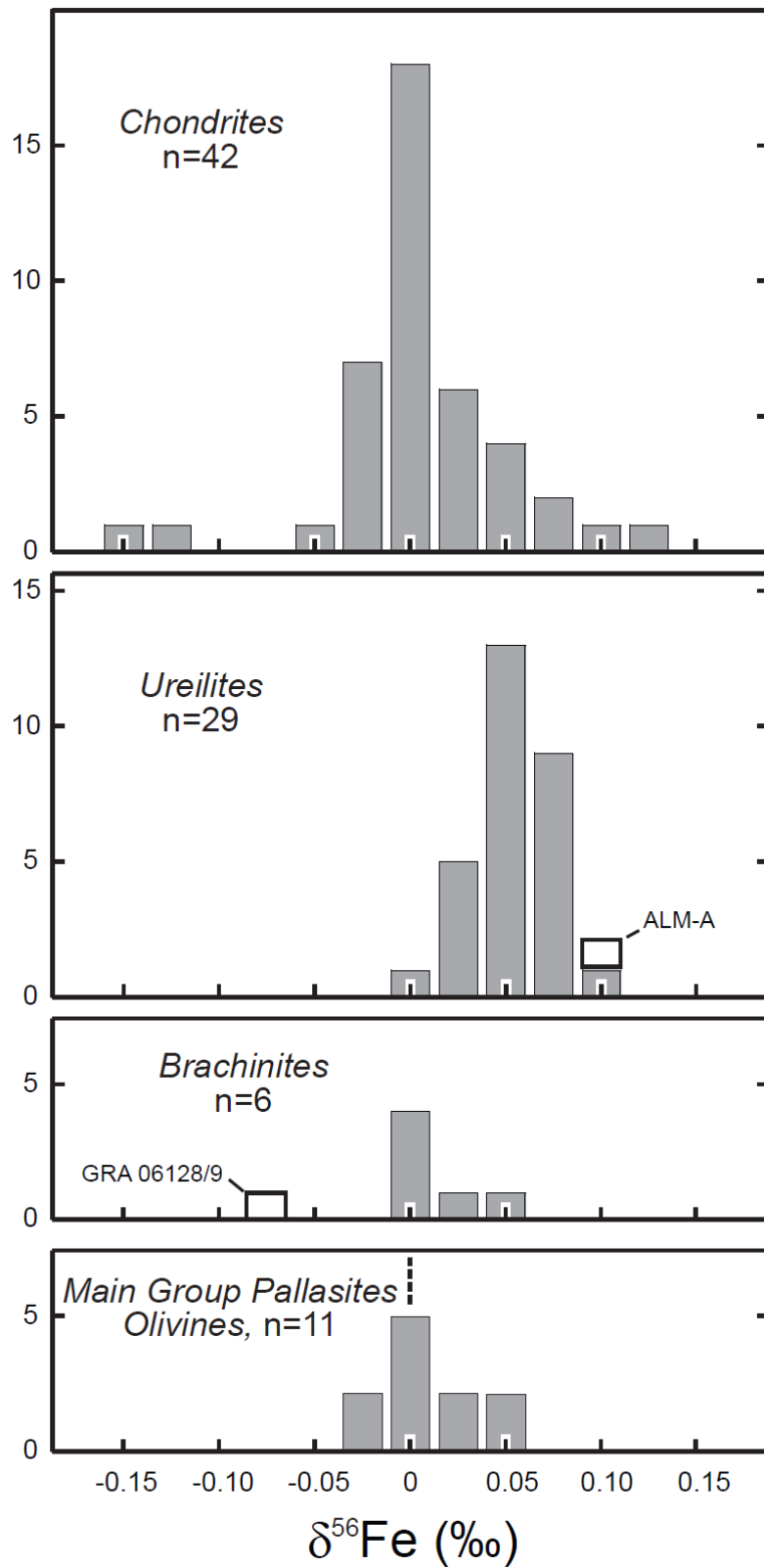
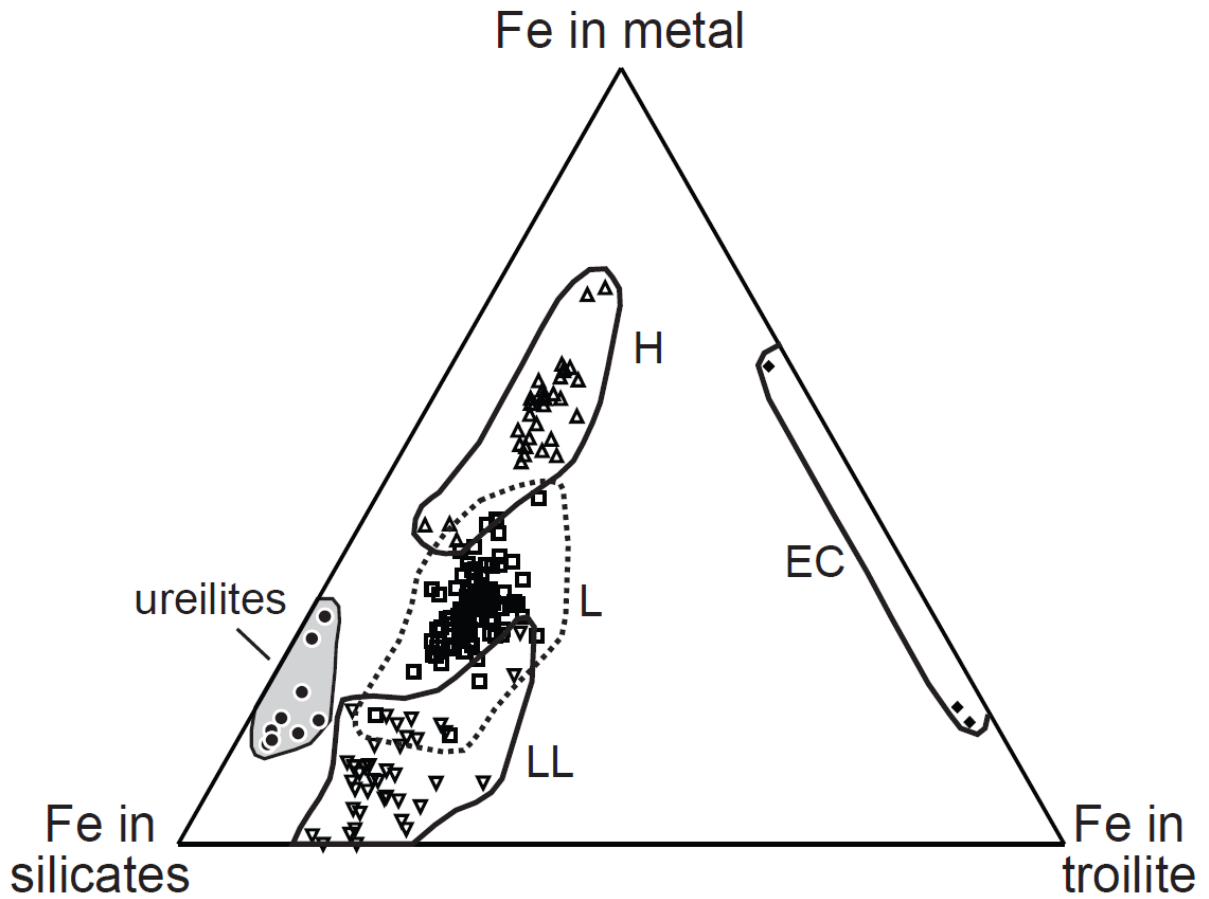
516  
517518  
519  
520  
521  
522  
523

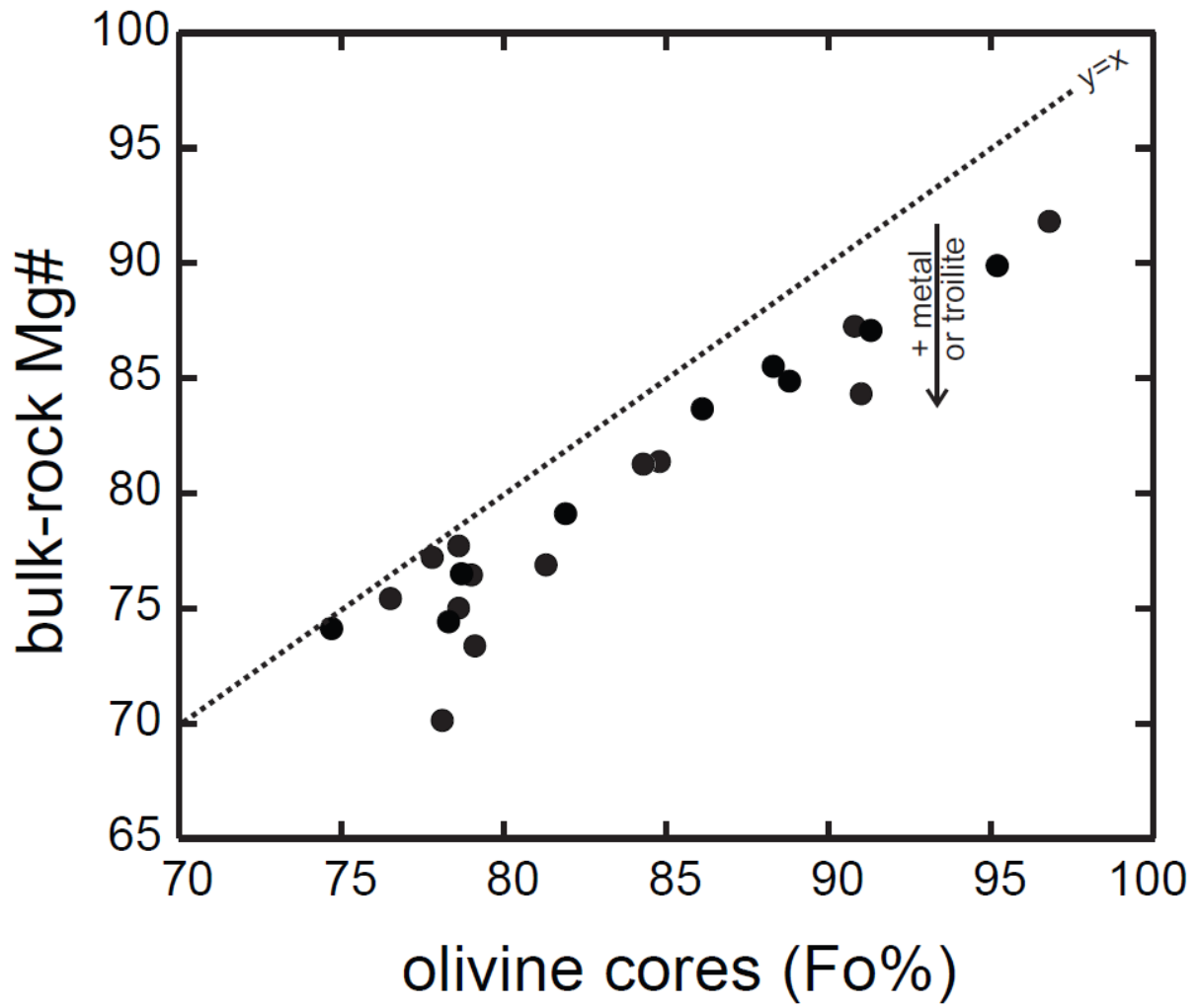
Figure 3. Iron isotope frequency distributions of chondrites (Craddock et al., 2013), ureilites and ALM-A, a ureilitic lava (this work), brachinites and GRA 06128/9, a brachinitic melt (Wang et al., 2014), and olivines from main group pallasites (Weyer et al., 2005).





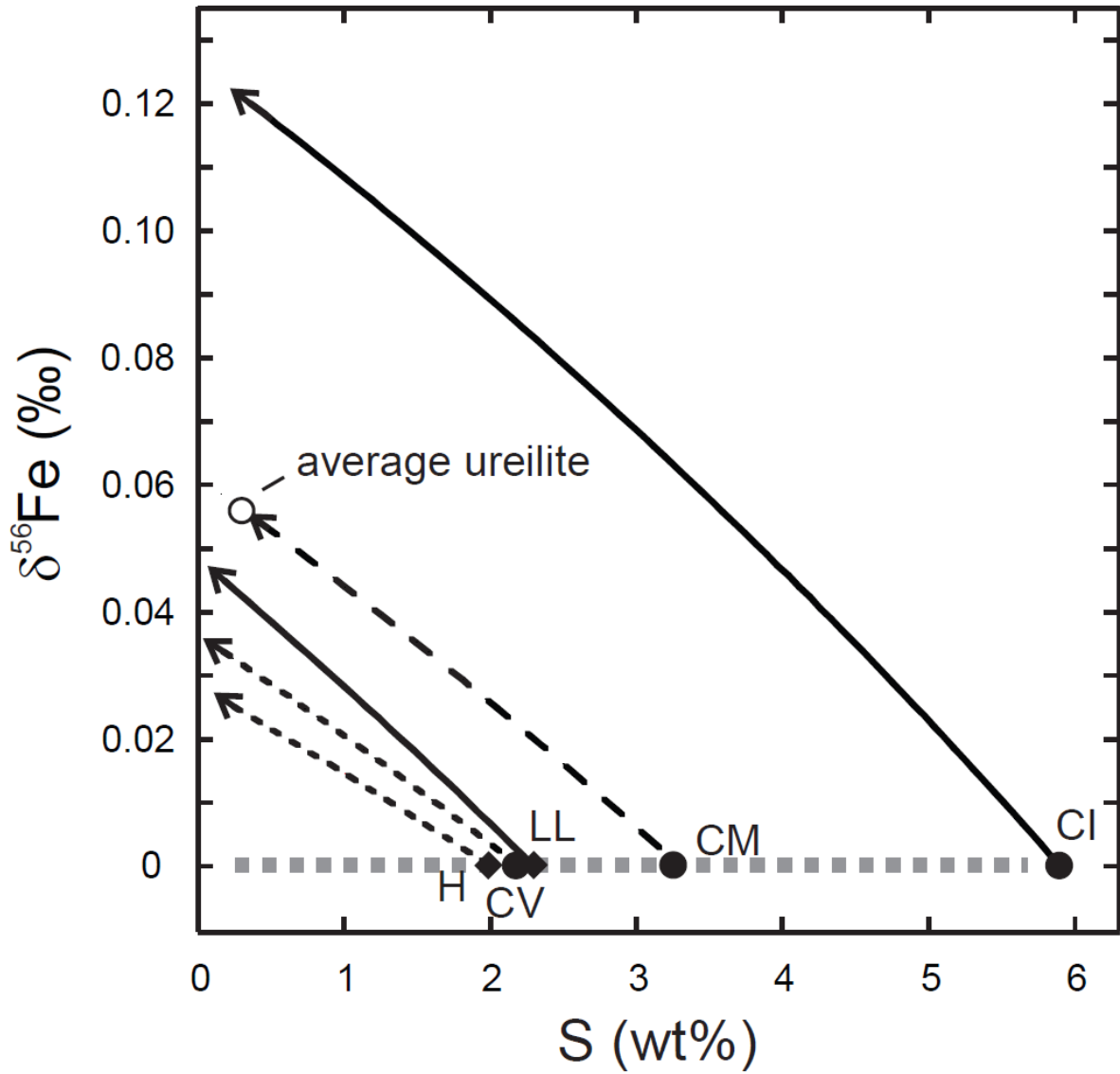
524  
 525  
 526  
 527  
 528  
 529  
 530

Figure 4. Ternary diagram showing the proportions of Fe hosted in the silicates, in metal and in sulfides for ureilites and non-carbonaceous chondrites (the proportions were estimated from the analyses compiled by Yanai et al., 1995).



531  
 532  
 533  
 534  
 535

Figure 5. Bulk-rock Mg# values vs. olivine-core compositions for the ureilites analyzed in Plouzané.



536  
 537  
 538  
 539  
 540  
 541  
 542  
 543  
 544

Figure 6. Evolution of the isotopic compositions of residual lithologies as a function of the extraction of a Fe-FeS melt with a eutectic composition. Starting assemblages have a  $\delta^{56}\text{Fe} = 0$  ‰ and the Fe and S contents of selected chondritic types (Wasson and Kallemeyn, 1988). The S abundance in the average ureilite is from Warren et al. (2006). A protolith with S and Fe abundances similar to average CM can account for the ureilite features, but this solution is not unique. Notice that the protolith of the ureilites is not a known carbonaceous chondrite (Warren, 2011).